AFRL-SN-RS-TR-1998-202
In-House Report
December 1998

NOISE IN OPTICAL AMPLIFIER AND MODE-LOCKED LASERS

James P. Theimer

Sponsored by
Ballistic Missile Defense Organization

APPROVED FOR PUBLIC RELEASE; DISTRIBUTION UNLIMITED.

AIR FORCE RESEARCH LABORATORY
SENSORS DIRECTORATE
ROME RESEARCH SITE
ROME, NEW YORK

This report has been reviewed by the Air Force Research Laboratory, Information Directorate, Public Affairs Office (IFOIPA) and is releasable to the National Technical Information Service (NTIS). At NTIS it will be releasable to the general public, including foreign nations.

AFRL-SN-RS-TR-1998-202 has been reviewed and is approved for publication.

APPROVED:

GREGORY J. ZAGAR
Chief, RF Photonics Branch
Sensors Directorate

FOR THE DIRECTOR:

ROBERT G. POLCE
Acting Chief, Rome Operations Office
Sensors Directorate

If your address has changed or if you wish to be removed from the Air Force Research Laboratory Rome Research Site mailing list, or if the addressee is no longer employed by your organization, please notify AFRL/SNDR, 25 Electronic Pky, Rome, NY 13441-4515. This will assist us in maintaining a current mailing list.

Do not return copies of this report unless contractual obligations or notices on a specific document require that it be returned.

REPORT DOCUMENTATION PAGE	Form Approved OMB No. 0704-0188

1. AGENCY USE ONLY *(Leave blank)*	2. REPORT DATE	3. REPORT TYPE AND DATES COVERED
	December 1998	In-House, Feb 97 - Sep 98

4. TITLE AND SUBTITLE

NOISE IN OPTICAL AMPLIFIER AND MODE-LOCKED LASERS

5. FUNDING NUMBERS

PE - 61102F
PR - 2304
TA - 07
WU - 02

6. AUTHOR(S)

James P. Theimer

7. PERFORMING ORGANIZATION NAME(S) AND ADDRESS(ES)

Air Force Research Laboratory/SNDR
25 Electronic Pky
Rome, NY 13441-4515

8. PERFORMING ORGANIZATION REPORT NUMBER

9. SPONSORING/MONITORING AGENCY NAME(S) AND ADDRESS(ES)

Ballistic Missile Defense Organization
7100 Defense Pentagon
Wash DC 20301-7100

Air Force Research Laboratory/SNDR
25 Electronic Pky
Rome, NY 13441-4515

10. SPONSORING/MONITORING AGENCY REPORT NUMBER

AFRL-SN--RS-TR-1998-202

11. SUPPLEMENTARY NOTES

AFRL Project Engineer: James P. Theimer/SNDR/(315) 330-4870

12a. DISTRIBUTION AVAILABILITY STATEMENT

APPROVED FOR PUBLIC RELEASE; DISTRIBUTION UNLIMITED.

12b. DISTRIBUTION CODE

13. ABSTRACT *(Maximum 200 words)*

This report describes the development of a simulation describing noise in mode-locked lasers, and some of the results of these simulations. The additive pulse mode-locking (APM) master equation is described and converted to a form compatible with previous work. Quantum noise and noise caused by the laser pump are described quantitatively and means of producing simulated noise are developed. The resulting quantum noise is compared to theory. Measures of laser noise and means of estimating the spectrum of a random signal are discussed. The measures of timing jitter and energy fluctuations from the simulation are found to agree well with an existing analytic model. Means for measuring random intensity noise (RIN) are developed. The spectrum of the output of a mode-locked laser simulation is analyzed using these tools. RIN over narrow frequency bands of the output is found to be well described by a randomly driven damped harmonic oscillator model. The effect of changing laser parameters was examined to identify strategies for developing low noise lasers. It was found that changes in the mode-locking parameter, cavity gain and loss had the greatest effect.

14. SUBJECT TERMS

mode-locked lasers, quantum noise, random intensity noise (RIN), optical amplifiers

15. NUMBER OF PAGES

48

16. PRICE CODE

17. SECURITY CLASSIFICATION OF REPORT	18. SECURITY CLASSIFICATION OF THIS PAGE	19. SECURITY CLASSIFICATION OF ABSTRACT	20. LIMITATION OF ABSTRACT
UNCLASSIFIED	UNCLASSIFIED	UNCLASSIFIED	UL

Abstract

This report describes the development of a simulation describing noise in mode-locked lasers, and some of the results of these simulations. The additive pulse mode-locking (APM) master equation is described, and converted to a form compatible with previous work. Quantum noise and noise caused by the laser pump are described quantitatively, and means of producing simulated noise are developed. The resulting quantum noise is compared to theory. Measures of laser noise and means of estimating the spectrum of a random signal are discussed. The measures of timing jitter and energy fluctuations from the simulation are found to agree well with an existing analytic model. Means for measuring random intensity noise (RIN) are developed. The spectrum of the output of a mode-locked laser simulation is analyzed using these tools. RIN over narrow frequency bands of the output is found to be well described by a randomly driven damped harmonic oscillator model. The effect of changing laser parameters was examined to identify strategies for developing low noise lasers. It was found that changes in the mode-locking parameter, cavity gain and loss had the greatest effect.

Table of Contents

Table of Figures

Table of Tables

1 Introduction

This report documents an Entrepreneurial Research (ER) project on noise in mode-locked lasers. The ability of photonic systems to achieve a variety of goals is limited by noise. The most obvious example of this is in communications networks. If optical pulses are used as bits in a communications network, the data rate of the system has to be large compared to the timing uncertainty of the source laser. Frequency fluctuations in the laser output will cause additional timing errors due to group velocity dispersion in optical fiber.

The major achievement of the effort has been the development of a computer model of laser noise. This was achieved by adding a random noise term to an existing laser model. There has been recent interest in using modes of a mode-locked laser as a comb of narrow bandwidth CW frequency sources. The results of the simulation have been analyzed to determine the predicted noise in the laser output in certain frequency bands.

The starting point for the work was a paper by Haus and Mecozzi[1]. They added random noise terms to a master equation describing pulse evolution in a mode-locked laser. Analytical techniques were used to derive expressions that describe the statistics of average pulse properties. These include fluctuations in pulse energy, mean wavelength, phase and timing jitter. This work consisted of justifying their noise model and, where necessary, extending it. Next, the art of running stochastic models on the computer had to be mastered. Experimentally measurable values had to be backed out of the simulation results.

2 Theoretical Model

2.1 Stochastic Master Equation

Haus and Mecozzi[1] addressed the problem of noise in mode-locked lasers by modifying the Additive Pulse Modulation (APM) master equation. APM theory has been applied to many laser systems, and has been described in detail[2,3,4]. I have used this model to describe a Cr^{4+}:YAG laser[5]. The master equation is similar to the Nonlinear Schrödinger Equation (NLSE) which I have simulated extensively to model pulse evolution in fiber lasers and fiber amplifiers[6,7,8]. The stochastic master equation is

$$T_R \frac{\partial}{\partial T} a(T,t) = \left[-\ell + g\left(1 + \frac{1}{\Omega_g^2}\frac{\partial^2}{\partial t^2}\right) + iD\frac{\partial^2}{\partial t^2} + (\gamma_3 - i\delta)|a(T,t)|^2 - \gamma_5 |a(T,t)|^4 \right] a(T,t) + T_R S(t,T).$$

Equation 2-1

The electric field envelope is represented by a(T,t), where t represents short-term time, and T is time on the order of the round trip time, T_R. The loss per round trip is given by ℓ, and the gain per round trip by g. The bandwidth of the amplifier is Ω_g, and D is the group velocity dispersion per round trip. The parameter γ_3 represents the mode-locking action, and γ_5 the saturation of this action, while δ gives the optical Kerr effect. Finally, S(T,t) is the noise source. The Kerr coefficient, δ, can be found by the equation

$$\delta = \frac{2\pi}{\lambda}\frac{L_K}{A_{eff}} n_2 .$$

Equation 2-2

where L_K is the length of the Kerr medium, and A_{eff} is the effective area of the beam in the medium. The wavelength of the laser light is λ. The parameter n_2 is the Kerr index. The effective index of the material is given by $n = n_0 + n_2 I$, where I is the intensity, and n_0 is the linear portion of the index of refraction. The dispersion D is related to

experimental quantities by $D \equiv \frac{1}{2} k'' L_d$, where k'' is the second order propagation coefficient and L_d is the length of the dispersive medium. Gain can be modified by gain saturation. This effect is given by $g(T) = \frac{g_0}{1 + \frac{1}{P_s T_R} \int dt |a(T,t)|^2}$ where P_s is the saturation power and g_0 is the small signal gain.

Equation 2-1 can be modified into a normalized form similar to that used in soliton simulations[9]. This was done by taking Equation 2-1 and dividing by $\frac{\beta_2}{T_0^2}$. The group velocity dispersion is given by β_2, and T_0 represents the pulse width. It will be more specifically defined in Equation 2-7. This yields

$$T_R \frac{T_0^2}{\beta_2} \frac{\partial}{\partial T} a(T,t) =$$
$$\frac{T_0^2}{\beta_2}\left[-\ell + g\left(1 + \frac{1}{\Omega_g^2}\frac{\partial^2}{\partial t^2}\right) + iD\frac{\partial^2}{\partial t^2} + (\gamma_3 - i\delta)|a(T,t)|^2 - \gamma_5 |a(T,t)|^4\right] a(T,t) + \frac{T_0^2}{\beta_2} T_R S(t,T)$$

Equation 2-3

If one substitutes $\tau = \frac{t}{T_0}$, and $\xi = \frac{\beta_2 T}{T_0^2 T_R}$ one derives

$$\frac{\partial}{\partial \xi} a(\xi,\tau) =$$
$$\left[-\ell + g\left(1 + \frac{1}{\tau_2^2}\frac{\partial^2}{\partial \tau^2}\right) + \frac{i}{2}\frac{\partial^2}{\partial \tau^2} + \frac{T_0^2}{\beta_2}\left\{(\gamma_3 - i\delta)|a(\xi,\tau)|^2 - \gamma_5 |a(\xi,\tau)|^4\right\}\right] a(\xi,\tau) + \frac{T_0^2}{\beta_2} T_R S(\xi,\tau)$$

Equation 2-4

where $\tau_2 = \frac{1}{\Omega_g T_0}$. The parameters ℓ and g are now in terms of dispersion lengths instead of round trips. A dispersion length is defined by $L_D = \frac{T_0^2}{\beta_2}$. The equation is further normalized by defining $u(\xi,\tau) = P_0^{1/2} a(\xi,\tau)$. The resulting equation is

$$\frac{\partial}{\partial \xi} u(\xi,\tau) =$$
$$\left[-\ell + g\left(1 + \frac{1}{\tau_2^2}\frac{\partial^2}{\partial \tau^2}\right) + \frac{i}{2}\frac{\partial^2}{\partial \tau^2} + \frac{P_0 T_0^2}{\beta_2}\left\{(\gamma_3 - i\delta)|u(\xi,\tau)|^2 - \gamma_5 P_0 |u(\xi,\tau)|^4\right\}\right] u(\xi,\tau) + \frac{T_0^2}{\beta_2\sqrt{P_0}} T_R S(\xi,\tau)$$

Equation 2-5

This equation becomes similar to the NLSE if we choose P_0 such that $\frac{P_0 T_0^2 \delta}{\beta_2} = 1$, and $\frac{P_0 T_0^2 \gamma_3}{\beta_2} = \Gamma$. This results in

$$\frac{\partial}{\partial \xi} u(\xi,\tau) =$$
$$\left[-\ell + g\left(1 + \frac{1}{\tau_2^2}\frac{\partial^2}{\partial \tau^2}\right) + \frac{i}{2}\frac{\partial^2}{\partial \tau^2} + (\Gamma - i)|u(\xi,\tau)|^2 + \frac{P_0^2 T_0^2 \gamma_5}{\beta_2}|u(\xi,\tau)|^4\right] u(\xi,\tau)$$
$$+ \frac{T_0^2}{\beta_2} T_R S(\xi,\tau)$$

Equation 2-6

This equation is similar to the NLSE, so soliton like trial solutions of the form

$$a(T,t) = \sqrt{P_0}\,\mathrm{sech}\left(\frac{t}{T_0}\right)$$

Equation 2-7

will be used.

2.2 Noise Terms

2.2.1 Quantum Noise

The power contributed by spontaneous emission into a mode is given by[10]

$$\frac{dP_{spont}}{dz} = \frac{N_2}{N_2 - N_1} g(\nu) h\nu B$$

Equation 2-8

where N_2, N_1 are the populations of the upper and lower levels of the state being excited. The bandwidth over which the noise is measured is B, and ν is optical frequency. Plank's constant is given by h. We will take the bandwidth as being $\Delta\omega/\pi$ and the line-shape function, $g(\nu)$ as being lorenzian[11,12]. This spectrum is generated by the stochastic Ornstein-Uhlenbeck process[13], which is generated by the Langevin equation[14]

$$\frac{E_{r,i}(t)}{dt} + \kappa E_{r,i}(t) = \sqrt{D} F(t)$$

Equation 2-9

where F(t) is a gaussisan random variable with a mean of zero and unit standard deviation. The real and imaginary components of the noise electric field are given by $E_{r,i}$. This process has a correlation function

$$\langle E_{r,i}(t), E_{r,i}(s) \rangle = \frac{D}{2\kappa} e^{-\kappa|t-s|},$$

Equation 2-10

and a lorenzian spectrum

$$F(\omega) = \frac{1}{\pi T_2} \frac{1}{(\omega - \omega_0)^2 + T_2^2}.$$

Equation 2-11

Values of D and κ, will be derived below. The line width is defined by the parameter T_2, where $\kappa = 1/T_2$. In order to have the same mean noise power as given in Equation 2-8 we need to have

$$\left\langle E_{r,i}(t), E_{r,i}(t) \right\rangle = \frac{DT_2}{2} = h\nu g\theta B dz$$

Equation 2-12

where $\theta = N_2/(N_2-N_1)$. Hence, using the bandwidth given above,

$$D = \frac{g\, h\nu\theta\, \Delta\omega\, dz}{\pi T_2}.$$

Equation 2-13

Since[10] $\Delta\omega = \frac{2}{T_2}$ Equation 2-13 reduces to

$$D = \frac{2gh\nu\theta dz}{\pi T_2^2}.$$

Equation 2-14

Equation 2-10 and the coefficients derived here can be used to compute random function with the correct statistics to represent spontaneous emission noise. The real and imaginary parts of x(T,t) are taken to be uncorrelated to each other.

Statistical measures of the resulting noise are shown in the following figures. Figure 2-1 shows a comparison of the expected to the measured spectrum. The measured spectrum here results from simply performing a discreet Fourier transform (DFT) routine on the data. More sophisticated methods will be described in section 4. The results show approximate agreement, though there is some problem at high frequencies. Figure 2-2 and Figure 2-3 show first and second order coherence respectively. Figure 2-2 has the correct exponential form. The abnormal shape at high frequencies appears to be eliminated by averaging over a greater number of points. Likewise the second order coherence appears to have the proper shape.

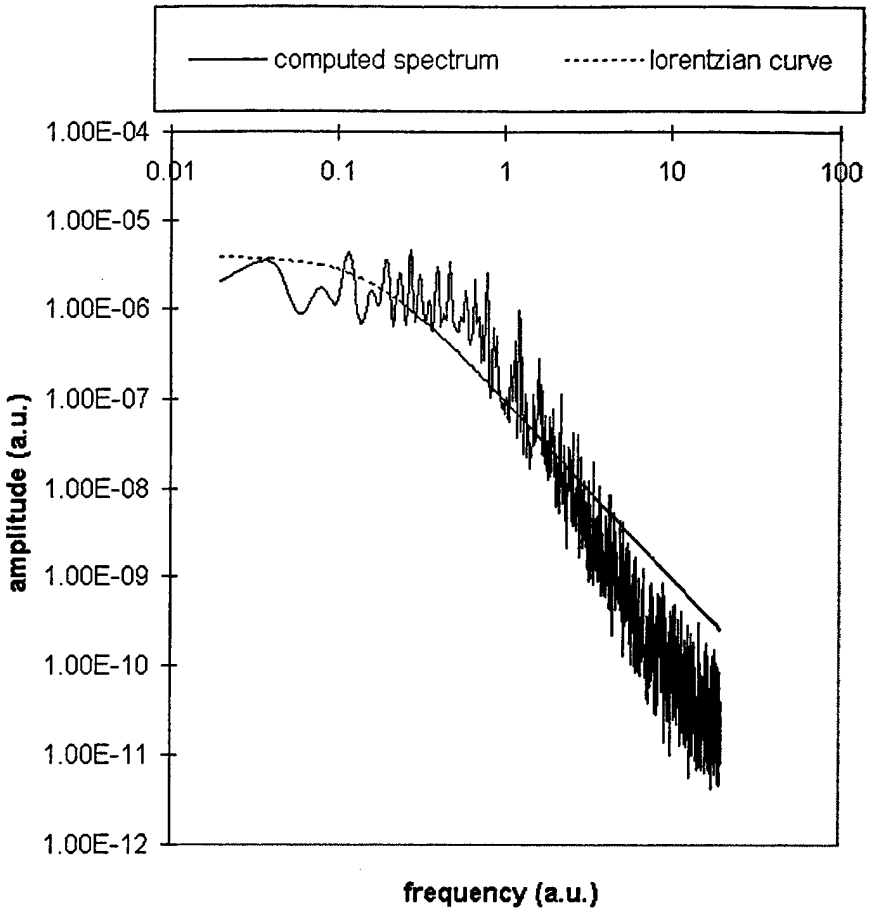

Figure 2-1 Comparison of the predicted to observed spectrum of the noise generation subroutine.

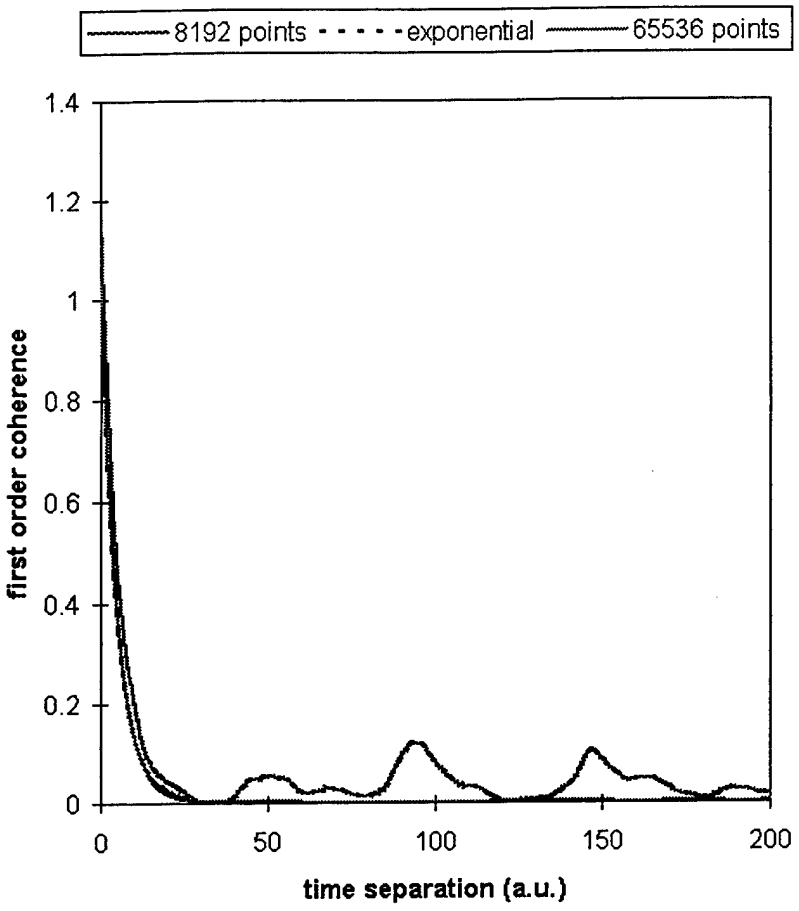

Figure 2-2 First order coherence of noise from the noise generation algorithm. The exponential curve is almost covered by the 65536 curve.

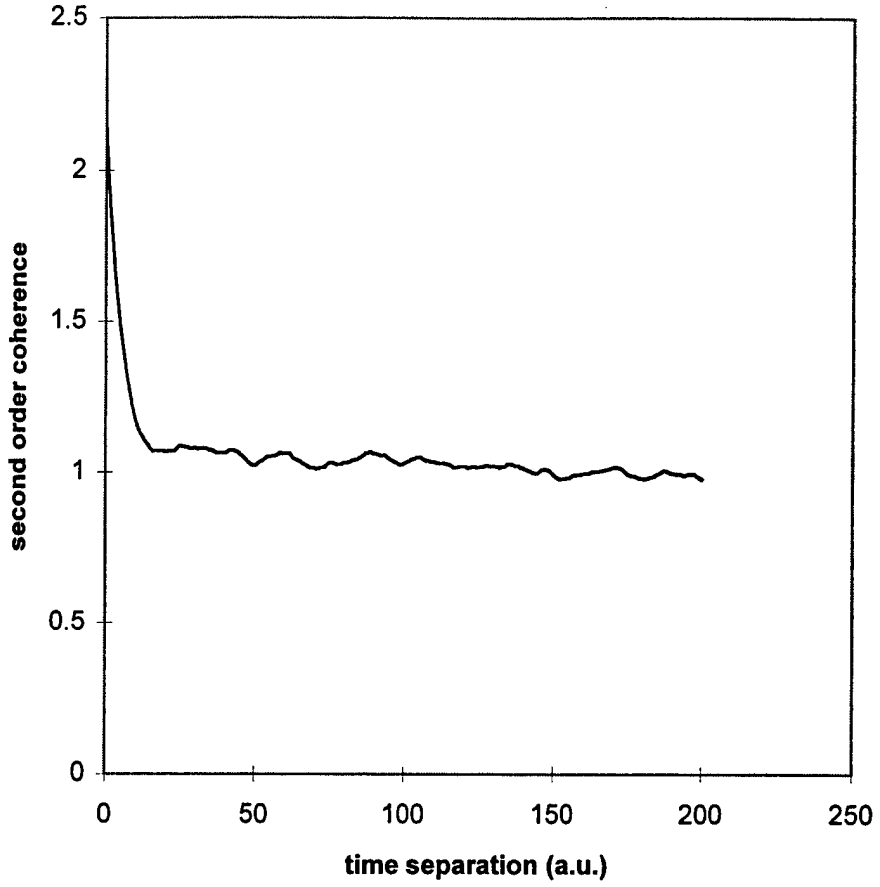

Figure 2-3 Second order coherence of the noise produced by the noise generation algorithm.

2.2.2 Pump Noise

As stated before, gain can be given as[15]

$$g(T,\nu) = \frac{g_0(\nu)}{1 + \frac{1}{P_s T_R}\int dt\,|a(T,t)|^2}$$

Equation 2-15

The small signal gain can be expressed as $g_0(\nu)=\sigma(\nu)N_0$, where σ is the emission cross section of the lasing transition, and N_0 is the unsaturated population inversion. For a four

level atom under conditions of weak pumping this inversion is given by $N_0 \cong t_{sp} N_a W$ where t_{sp} is the spontaneous emission lifetime, N_a is the lasing atom density and W is the probability density for the absorption of pump light. This is in turn given by $W = \sigma_p \phi_p$, where σ_p is the absorption cross section of the pump light and ϕ_p is the pump photon flux. Consequently the small signal gain can be expressed as

$$g_0(\nu) = \sigma(\nu) t_{sp} N_a \sigma_p \phi_p .$$

Equation 2-16

The mean pump intensity over a period of time, dt, is given by $\overline{m} = \overline{\phi}_p \, dt$. For a thermal source the pump photon number has a Poison distribution, so it has a variance [12]

$$(\Delta m)^2 = \overline{m}.$$

Equation 2-17

This effect can be included in the numerical simulation by computing the mean pump flux, using a Poisson random number generator to compute the flux for each time step, and then Equation 2-16 to compute the small signal gain for the step.

2.3 Simulation Methods

Equation 2-7 was numerically integrated using the Split Step Fourier Transform method. This method has been extensively discussed elsewhere [9,16,17]It can be considered to be an example of a spectral algorithm for solving a partial differential equation[18]. Spontaneous emission noise was added using Equation 2-9 and varying the gain according to Equation 2-16 and Equation 2-17.

2.4 Noise Background

This section will define Relative Intensity Noise (RIN). Noise in single mode lasers has been extensively studied[19,12,20,21]. Noise can cause fluctuations in both the intensity and phase of a single mode laser. Relative intensity noise (RIN) is the principle focus of the work described here. RIN is defined as

$$RIN = \frac{S_P(\omega)}{\overline{P}^2}.$$

Equation 2-18

where the spectral density is defined as

$$S_P(\omega) = \int_{-\infty}^{\infty} \langle \delta P(t+\tau)\, \delta P(t) \exp(-i\omega\tau)\, d\tau \rangle$$

Equation 2-19

where $\delta P(t) = P(t) - \overline{P}$. The power of the laser is given by P(t), and the mean power by $\overline{P}$. This can be used to obtain the mean squared deviation

$$\langle [\delta P(t)]^2 \rangle = \int_0^{\infty} S_p(f) df$$

Equation 2-20

3 RIN caused by spontaneous emission

This section discusses intensity fluctuations caused by spontaneous emission. The noise was added to the model as described in Section 2.2.1. The results of the model can be analyzed in a number of ways. Predictions of average pulse phenomena can be produced. These are useful as they can be compared to an analytic theory.

3.1 Haus-Mecozzi predictions

Haus and Mecozzi predicted that timing jitter would vary as[22]

$$\left\langle \left| \Delta t(T - T_0) - \Delta t(T_0) \right|^2 \right\rangle = \frac{4D^2}{T_R^2} D_{p,qn} \tau_p^3 \left[\frac{T}{\tau_p} - 1 + \exp\left(\frac{-T}{\tau_p} \right) \right].$$

Equation 3-1

The diffusion coefficient due to quantum noise, $D_{p,qn}$ is given by

$$D_{p,qn} = \frac{2}{3 w_0 T_0^2} \theta \frac{2g}{T_R} h\nu$$

Equation 3-2

and the relaxation time τ_p by

$$\tau_p = \frac{3 T_0^2 T_R}{4 g T_2^2}$$

Equation 3-3

where w_0 is the pulse energy. For a hyperbolic secant pulse, the energy is $w_0 = 2 P_0 T_0$. The data for this calculation are summarized in Table 1. The saturated gain, g, when computed, is 0.138. Hence the relaxation time is $\tau_p = 2.037 \times 10^{-6}$ sec, where T_R should be replaced with T_D Equation 3-3. The quantum noise diffusion coefficient is $D_{p,qn}$. These data were used because they describe a laser which I had simulated in great detail in the past[5].

D (fs^2/round trip)	2675
T_R (sec)	6.67×10^{-9}
w_0 Joules	6.93×10^{-8}
T_0 (sec)	72.86×10^{-15}
g_0 (1/dispersion lengths)	0.059
T_D (sec/dispersion lengths)	8.33×10^{-9}
$h\nu$ (joules)	1.28×10^{-19}
T_2 (sec)	34.4×10^{-15}

Table 1 Typical laser physical parameter values.

Equation 2-6 was numerically integrated as described in Section 2.3. The results are shown in Figure 3-1. The "theory" curve plots the results of Equation 3-4.

$$\left\langle \left| \Delta t\left(\frac{Z-Z_0}{T_D}\right) - \Delta t\left(Z_0\right) \right|^2 \right\rangle = \frac{4D^2}{T_R^2} D_{p,qn} \tau_p^3 \left[\frac{Z}{\tau_p T_D} - 1 + \exp\left(\frac{-Z}{\tau_p T_D}\right) \right].$$

Equation 3-4

In this equation certain units have been changed. Notably the separation is given in units of dispersion lengths, and the magnitude of the timing jitter is in units of T_0^2. The curves for series 1, 2, and 3 represent 3 different sets of parameters for the degree of numerical detail in the calculation. The agreement for between the simulations and the theory is within 10%. The step size in the calculation was 0.001 dispersion lengths. The pulse was propagated for 400,000 steps. To generate an accurate estimate of pulse jitter one had to average over all 400,000 steps. Curves based on averaging over only 400 steps had the correct slope, on the log-log plot, but their y intercepts disagreed between each other by an order of magnitude. The excellent agreement between theory and simulation in this case gives confidence that the simulation is working well.

Similar analysis can be done with energy fluctuations. The correlation function of these is described by

$$\left\langle w\left(T+T_0\right) w\left(T_0\right) \right\rangle = \frac{\tau_w}{2} D_{w,qn} \exp\left(\frac{-|T|}{\tau_w}\right)$$

Equation 3-5

where the relaxation time is given by

$$\frac{1}{\tau_w} = \frac{2\left(g_s - \gamma_3 A_0^2 + \gamma_5 A_0^4\right)}{T_D}$$

Equation 3-6

and g_s by

$$g_s = \frac{2 g_0 T_0 A_0^2}{P_s T_R \left(1 + \frac{2 T_0 A_0^2}{P_s T_R}\right)^2}.$$

Equation 3-7

The diffusion coefficient of interest is

$$D_{w,qn} = 4w_0 \frac{2g}{T_R} h\nu .$$

Equation 3-8

The spectrum of the energy fluctuations is given by

$$\left\langle \left| \delta w(\Omega) \right|^2 \right\rangle = \frac{\left\langle \left| S_p(\Omega) \right|^2 \right\rangle}{\Omega^2 + \frac{1}{\tau_w^2}},$$

Equation 3-9

where

$$\left\langle \left| S_w(\Omega) \right|^2 \right\rangle = D_{w,qn} .$$

Equation 3-10

These predictions are compared to the simulation in Figure 3-2. The predictions here are not as accurate as in the last case, however, there is rough agreement. A possible explanation for the details in the simulation will be discussed in the next section.

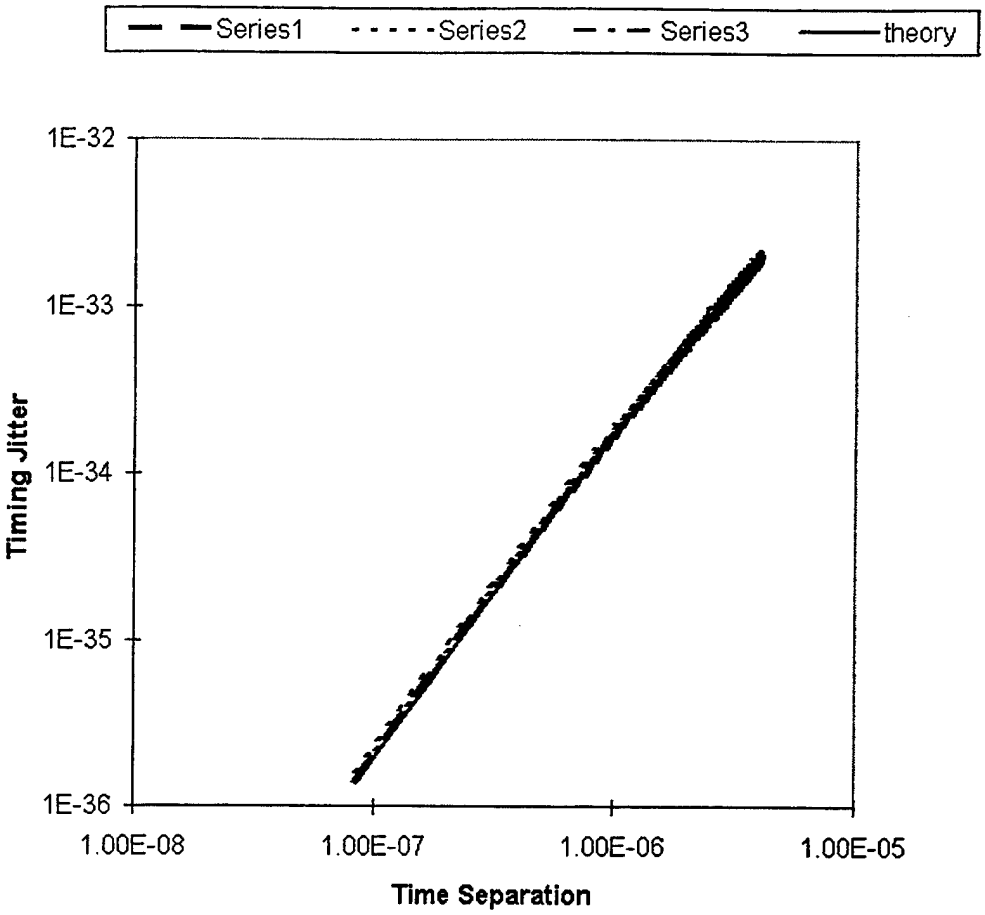

Figure 3-1 Comparison of theory to a simulation of the timing jitter. The different series had different numerical step sizes, showing that the results were not highly sensitive to numerical parameters.

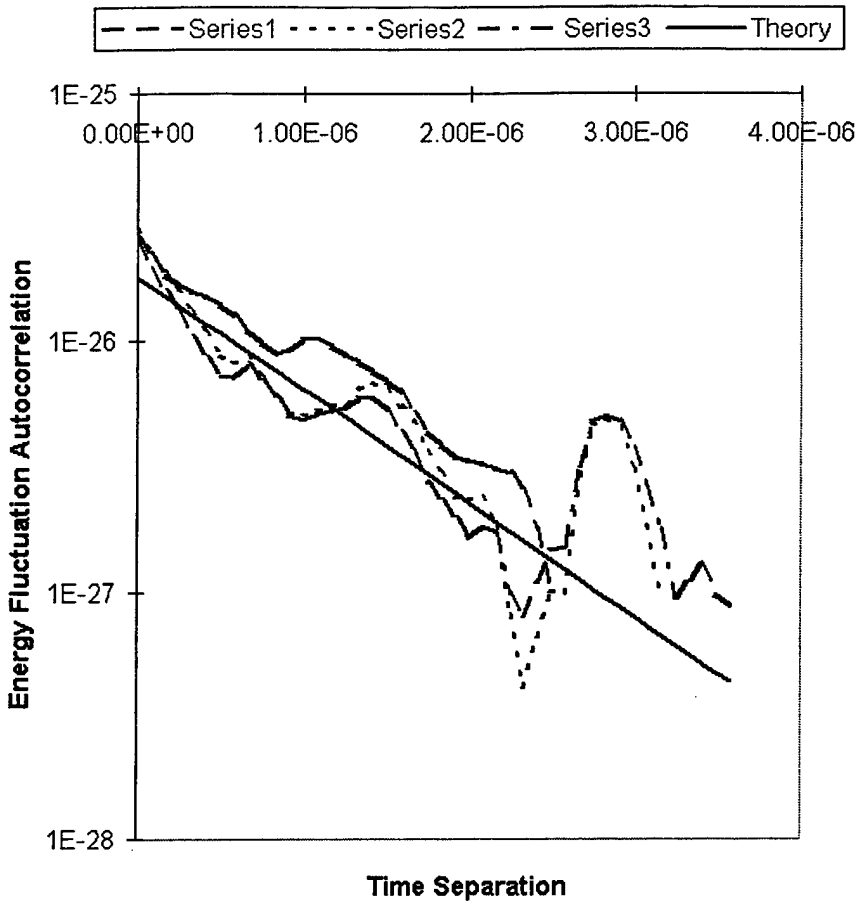

Figure 3-2 Comparison of theory and simulation of energy fluctuations. The different series resulted from simulations with different step sizes, or window sizes.

4 Spectral Estimation

The simulations developed for this project resulted in long sets of random data. To measure RIN it was necessary to estimate the underlying spectrum of the noise. Spectral estimation is discussed in a number of standard textbooks[23,24]. The algorithms here were adopted from Press et al.[25]. These techniques are necessary due to the finite length of the data series, and the fact that the data is only sampled at discrete points in time. For these reasons one cannot simply Fourier transform the data.

The windowing technique uses weighting functions in conjunction with the discrete Fourier transform. The data set is divided up into a large numbers of windows, and the results of the windows are averaged. Using a long window allows for picking up very narrow data features. However it also means that one can only average over a smaller number of windows. This results in greater uncertainty in the precision of each point. In contrast the Maximum Entropy method works by fitting a certain number of poles to the Z-transform of the data. This method tends to work well for strongly peaked data. Fitting to a larger number of poles will find more real poles, but can also result in spurious results.

Figure 4-1, and Figure 4-2 show the result of applying these techniques to synthetic data generated by means described above. The theoretical frequency spectrum of the noise is also shown. In Figure 4-1 we see that both of the techniques seem to correctly estimate the shape of the curve. The windowing technique has a spurious peak at low frequencies. Both techniques seem to show elevated noise at high frequencies. This could be evidence of a problem in the noise generation method, though the problem occurs when the noise is three orders of magnitude down from the peak. Figure 4-2 shows the results of fitting to more poles. The basic result appears to be to pick up more noise. The 20 pole results appear to give reasonable results, so this was adopted for data analysis.

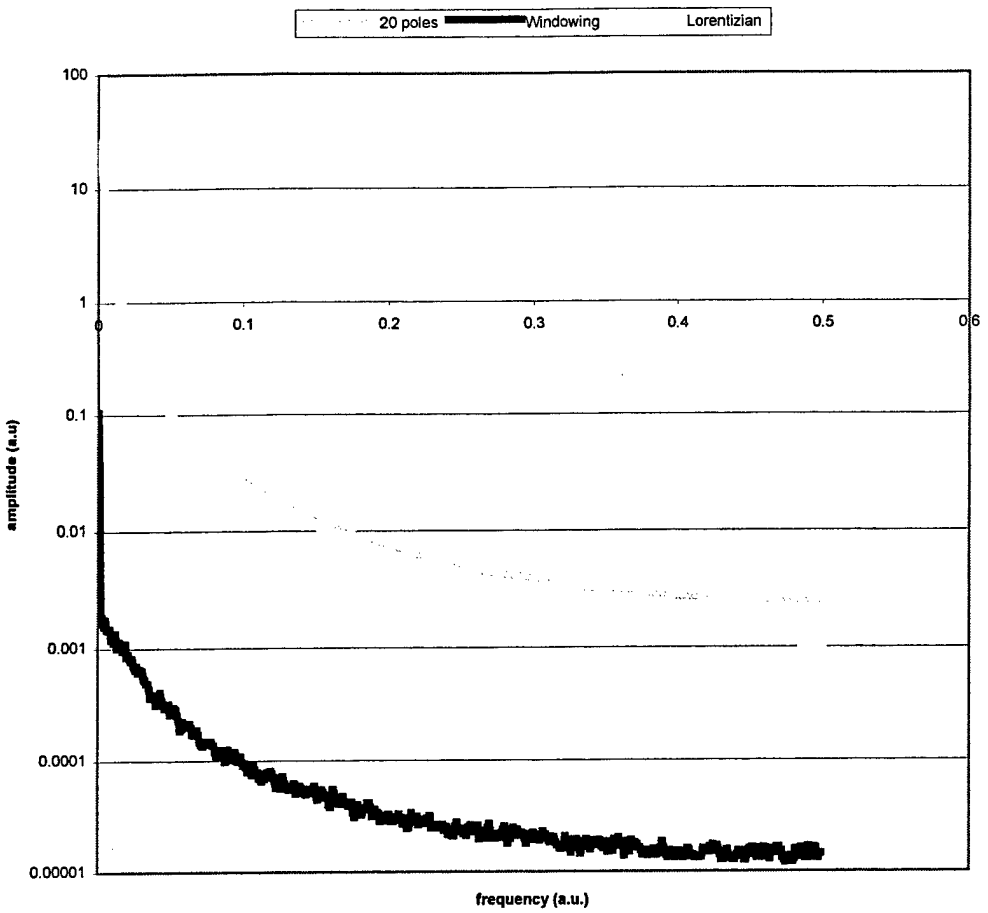

Figure 4-1 Comparison of the results of using the all-poles and the windowing spectral estimation methods.

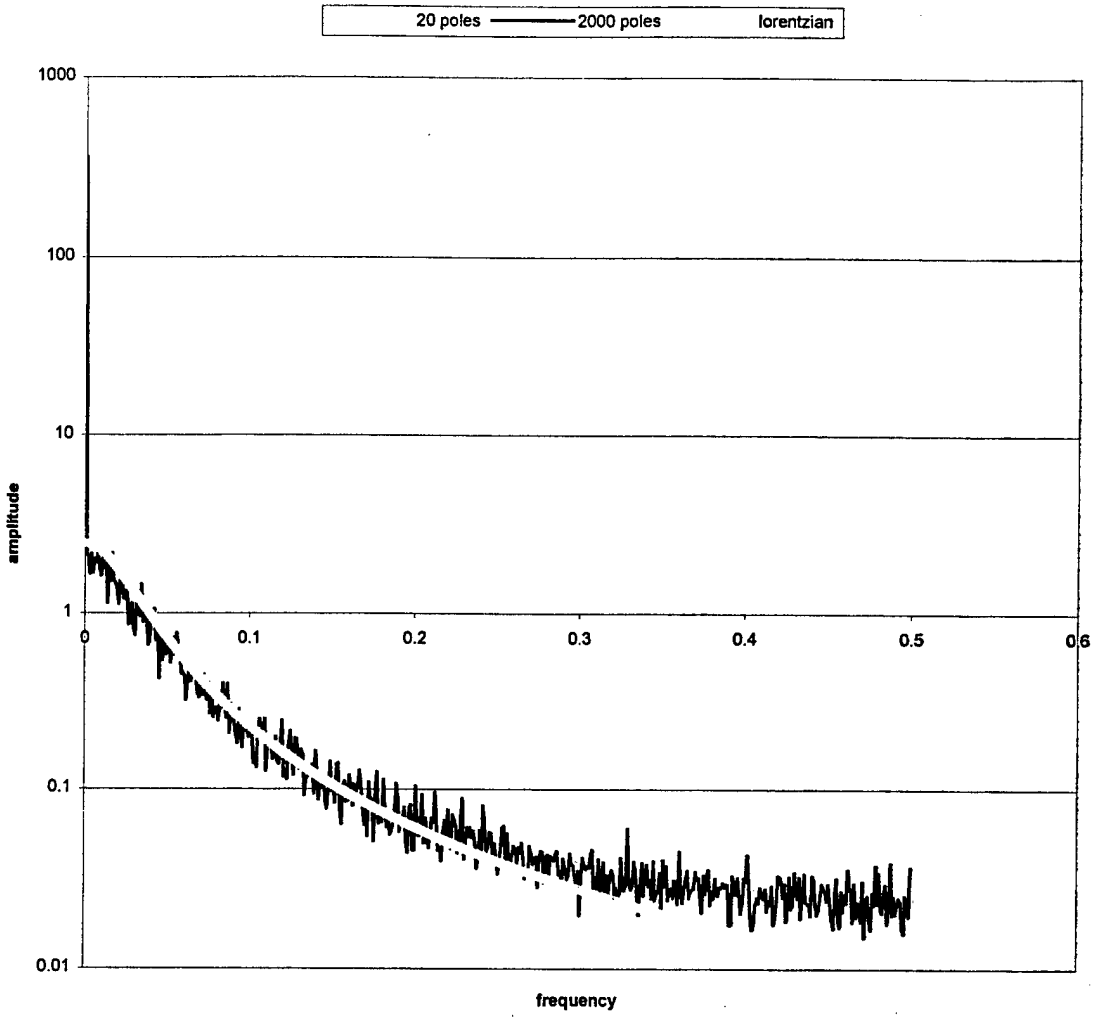

Figure 4-2 Comparison of using 20 and 2,000 poles for spectral estimation.

5 Simulation Results

5.1 Simulation Technique and RIN Spectrum and Noise Model

5.1.1 Simulation Technique

The pulse information is stored in the form of function $u(\xi,\tau)$. A time window much wider than the width of the pulse was used. For this reason it was reasonable to convert this function to the frequency domain by using the FFT algorithm. This left a function of the form $u_f(\xi,\nu)$, where ν represents the frequency components of the pulse. This was converted to the normalized form

$$F(\xi,\nu_i)=\frac{u_f(\xi,\nu_i)-\langle u_f(\xi,\nu_i)\rangle_\xi}{\langle u_f(\xi,\nu_i)\rangle_\xi}.$$

Equation 5-1

The frequency spectrum of $F_f(\Omega,\nu_i)$ was determined using the spectral estimation techniques described in section 4. The slowly varying frequency components are given by Ω. The FFT results in estimates of the RIN over a number of frequency ranges, or Bins. These are distinguished by the index in the variable ν_i.

Pulse energy in all cases was maintained at about 1.05 in normalized units. This strategy simplified drawing comparisons between results produced by different laser operating parameters. For a given set of parameters the gain was adjusted to achieve this energy. I started the simulation with a trial pulse and let the pulse shape settle down to its final form. In practice there were many problems that needed to be overcome. If the gain became too large the pulse would be unstable and collapse. Ultimately the simulation would start from noise, but it would form two smaller pulses, rather than one big one. When I discussed this with a colleague to compare this with experimental observations, I found out that if the gain in the laser described by the simulations was increased too much, it would produce multiple pulses in the cavity[26]. Apparently this instability is an actual feature of the system, and not simply a numerical artifact.

A second problem was determining when the simulation had settled down to equilibrium. This was done by plotting the function $F(\xi,\nu_l)$ for the DC frequency bin. An example of this is shown in Figure 8. The function is a damped sine wave for the first part of the simulation, until it becomes dominated by noise. At this point the function appears to be a sine wave with a random modulation as shown in Figure 5-2. The period of the oscillations is approximately 33 dispersion lengths. If the oscillation of the pulse is linked to soliton shaping mechanisms, one would expect the period to be similar to this.

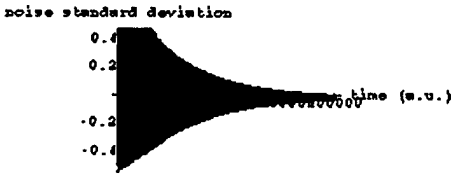

Figure 5-1 The simulation settles down from starting conditions into a randomly modulated sine wave.

Figure 5-2 A detailed view of normalized energy fluctuations of the central frequency bin.

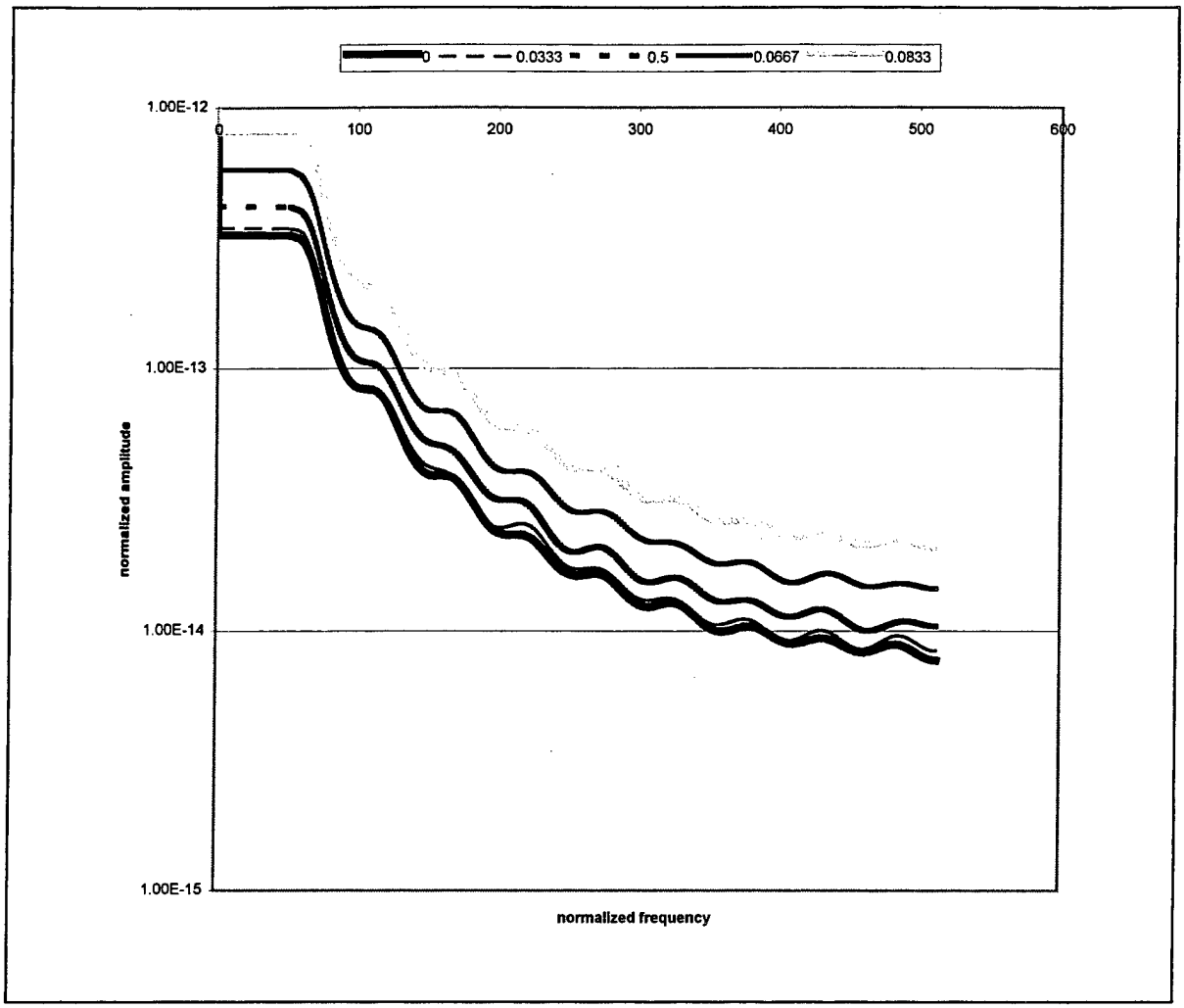

Figure 5-3 Shows the variation in RIN for increasing bin frequency.

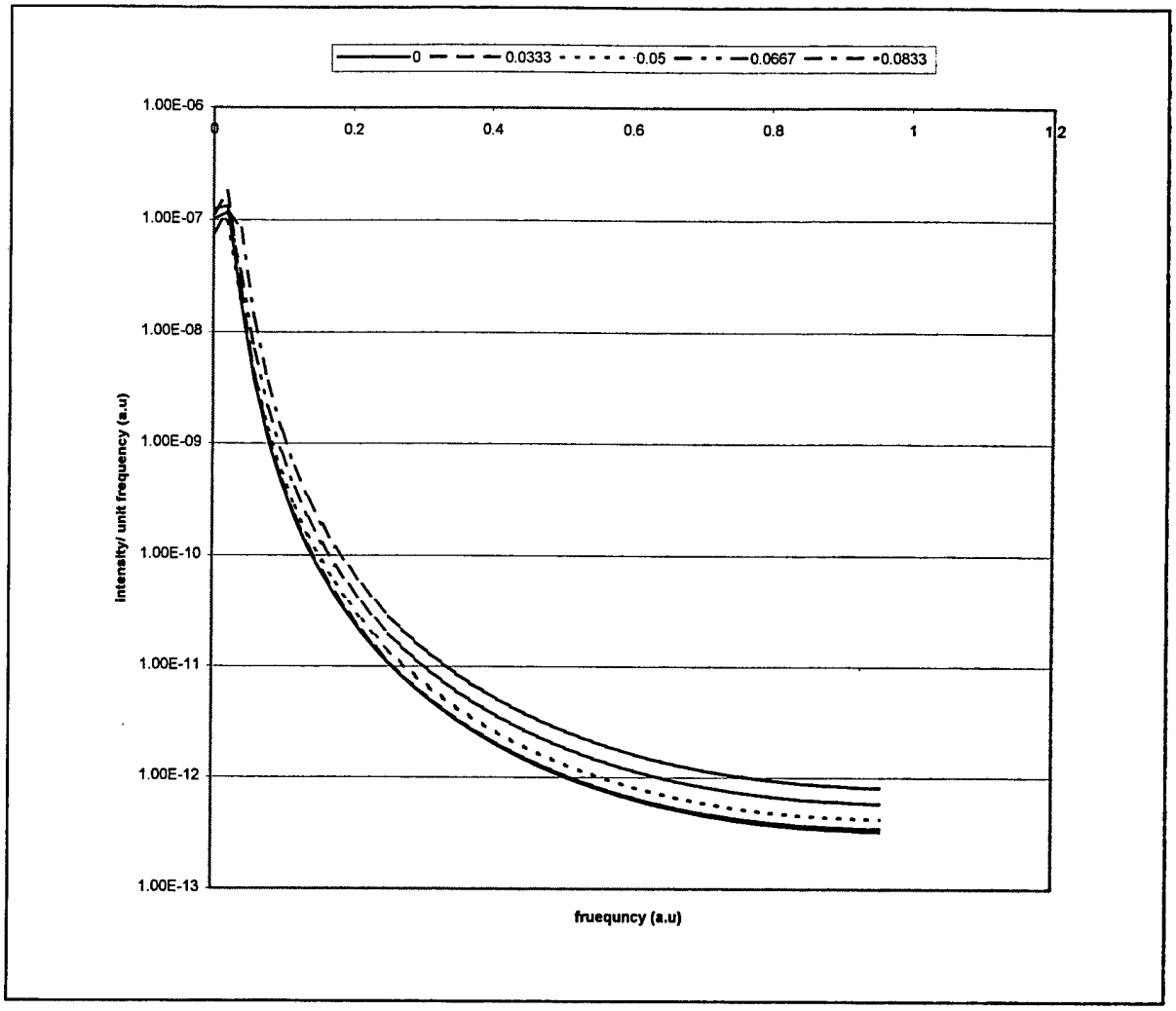

Figure 5-4 Shows the variation in RIN with Bin frequency. This figure concentrates on the low frequencies, where RIN changes rapidly.

An example of the resulting frequency spectra can be seen Figure 5-3. In general higher frequencies show greater RIN. Since the intensity of the pulse falls off with frequency, this could be explained by a constant fluctuation magnitude being divided by a smaller intensity in Equation 5-1. The curve shows a dramatic peak at low frequencies, as shown in Figure 5-4.

5.1.2 Noise Model

One would like to gain physical insight into the nature of the noise. In Figure 5-5 one sees the shape of the central frequency RIN curve. Equation 3-9 shows the expected fluctuation spectrum of the pulse energy, which is a reasonable guess for the spectrum of

the noise in each frequency bin. This noise has a lorenzian curve. The relaxation time was computed by using Equation 3-6. The amplitude was determined by using Equation 3-9. This approach doesn't predict the low frequency spike. The other model is described as bound motion in Reference 23. This model results from a stochastic differential equation similar to that which gives the lorenzian spectrum, except that it incorporates a restoring force. In practice, there are two restoring forces in the computer model, which don't appear in the analytic theory. The simulation includes the γ_5 term, which tends to control the pulse energy. Additionally, in the analytic theory the saturated gain is treated as a static quantity, while in the simulation, it is continuously recomputed. As in a CW laser, this also tends to clamp the energy to an equilibrium value. The lorenzian spectrum results from a stochastic differential equation

$$\frac{dx}{dt} + \frac{f}{m}x = \frac{1}{m}F(t).$$

Equation 5-2

In contrast bound motion has the form

$$\frac{d^2x}{dt^2} + \frac{f}{m}\frac{dx}{dt} + \frac{c}{m} = \frac{1}{m}F(t).$$

Equation 5-3

The coefficient f represents a dissipative force, and c is the restoring force. The forcing function is assumed to be white noise of the form $S_F(\omega) = 2kTf$. The resulting spectrum is

$$S_x(\omega) = \frac{f}{\left(c - m\omega^2\right)^2 + f^2\omega^2}.$$

Equation 5-4

The autocorrelation function

$$R_x(\tau) = \frac{kT}{c}e^{-\alpha|\tau|}\left[\cos(\beta\tau) + \frac{\alpha}{\beta}\sin(\beta|\tau|)\right]$$

Equation 5-5

where $\alpha=f/2m$, and $\alpha^2+\beta^2=c/m$.

Equation 5-3 can be justified on a somewhat more rigorous basis. Equation 3-9 is derived from a differential equation[1]

$$T_R \frac{\partial}{\partial T}\Delta w = \frac{1}{\tau_w}\Delta w + T_R S_w(w).$$

Equation 5-6

If one assumes that there is some additional effect, such as pulse reshaping, which is not a function of the current state of the system alone, then one would need to add an additional term to Equation 5-6, and it will become

$$T_R \frac{\partial}{\partial T}\Delta w = \frac{1}{\tau_w}\Delta w + T_R S_w(w) + \int_{-\infty}^{t} \Delta w\, h(t')dt',$$

Equation 5-7

where h(t) is the memory function. If one takes the derivative of Equation 5-7, one obtains

$$T_R \frac{\partial^2}{\partial T^2}\Delta w = \frac{1}{\tau_w}\frac{\partial}{\partial T}\Delta w + T_R S_w(w) + \text{const.},$$

Equation 5-8

which is an equation of the form of Equation 5-3. This result suggests that one could estimate the damping function form τ_w, and estimate the constant term from the period of the oscillation.

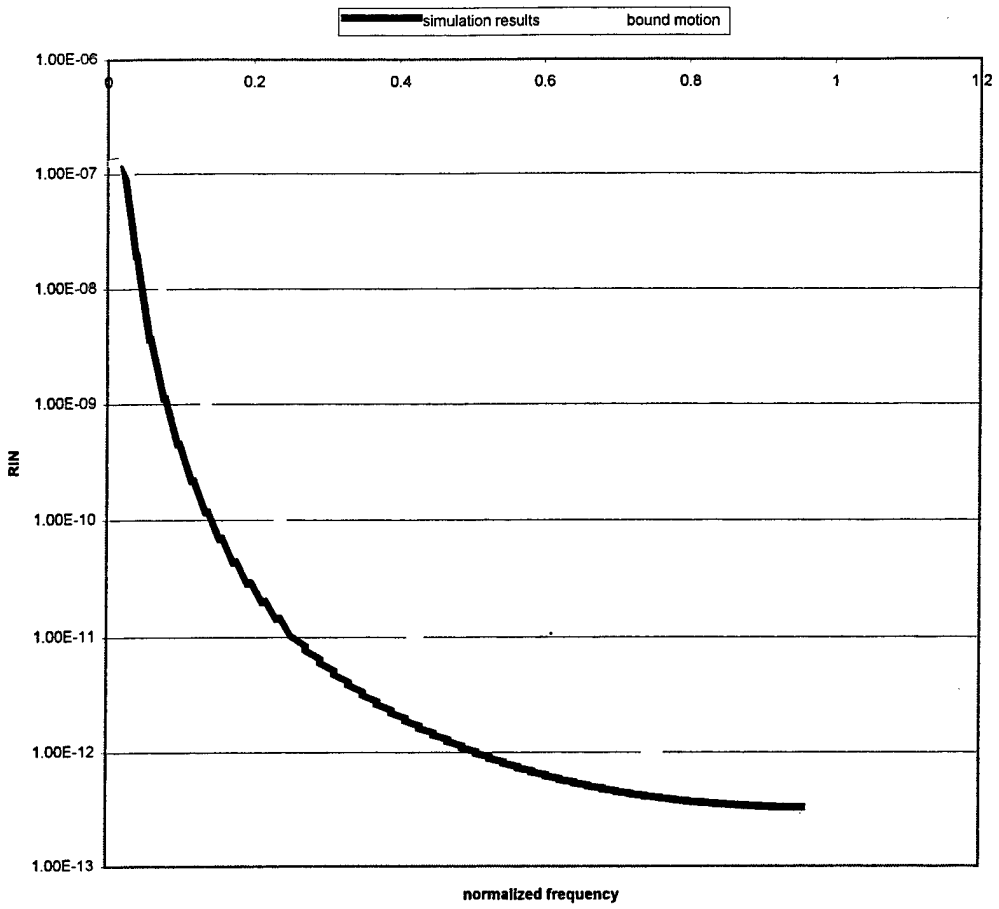

Figure 5-5 Compares central mode RIN to various models.

The form of the autocorrelation function is at least suggestive of Figure 5-1 which shows how the simulation settles down from starting conditions. This model will be examined further in a later section. By comparing Equation 5-8 and Equation 5-5 the value of α could be equated to $1/\tau_w$. The period was estimated from Figure 5-2, and this was used to estimate β. The noise magnitude, 2kT, was estimated by Equation 3-8. The resulting curve approximates the simulated data. When the results from the lorenzian curve, and the bound motion curve are combined, they resemble the simulated results over a wide range. The integrated area under the combined curve and the lorenzian differ by less than 10%. It appears that the bound motion model is a reasonable estimate of the central noise spike. It does not predict the high frequency results, which are better

predicted by the lorenzian model. The high frequency noise only accounts for a small percentage of the total, so this is not a grave problem.

5.2 *Effect of Changing Laser Parameters*

One would like to gain further knowledge of the nature of the memory function introduced in the last section. In addition, one main intent of this project was to explore the sensitivity of laser noise to experimentally controllable laser design parameters. In practice this proved to be quite difficult. It was found that when γ_5 was set to zero, or when the laser loss was set to too low a value, the simulation was not stable. When γ_5 was eliminated, for instance, the noise of the central frequency bin was an exponential growing sine wave, rather than the exponentially damped one, as shown in

. Similar results appeared when the loss was reduced. The noise total fluctuation magnitude could be nearly as large as the mean magnitude.

In practice it was found that one could vary the mode-locking coefficient, and the amplifier bandwidth. The effect of changing these over a wide range was explored. To simplify the results, the RIN was summarized as the area under the RIN curve. We know from Equation 2-20 that this is equal to the variance, or the autocorrelation function with no time delay. From Equation 5-5 we see that this is equal to $\frac{kT}{c}$. The parameter kT could be adjusted. This corresponds to $D_{w,qn}$. It can be reduced by lowering the pulse energy, gain, or photon energy. Often these are not open to adjustment. These results run contrary to the observation from the simulations that decreasing loss, and hence gain, tended to increase the size of the fluctuations. It appears that loss must effect the parameter c in some powerful way.

The parameter c is not well understood. As mentioned above the value used in calculations was obtained from the period of the oscillations of RIN. What effects control the period of these oscillations? It was observed above that the period is on the order of that expected for soliton shaping mechanisms. Soliton effects tend to take place over length scales of a dispersion length. A pulse will tend to evolve into a soliton over tens of dispersion lengths. For this reason the 33 dispersion length figure derived above is plausible. The parameters that effect this are linear dispersion, material nonlinearly,

and pulse energy. Hence, achieving low fluctuations requires low pulse energies, low dispersion, and low nonlinearities. This leads to little pulse shaping and hence broad pulses. Since such parameters as the pulse energy, cavity dispersion, and nonlinearity are often hard to control, or are set by application requirements, it may be hard to control the parameter c by altering them.

Some conclusions about the nature of the memory function, and the resulting fluctuation magnitude can be derived from the simulation results and knowledge of APM laser functions. Loss, and the mode-locking effect work together to form the pulse in these lasers. Less intense parts of the pulse receive less gain from the mode-locking element. These parts of the pulse will see a net loss as they go through the laser cavity. A laser with high loss and a powerful mode-locking device will have a more powerful mode-locking effect, and the pulse will more rapidly evolve into its final state. This qualitatively explains the observation that these are related to a higher oscillation frequency. In particular, it may be that small changes in cavity loss have a large impact on the period of the energy oscillations. This could explain the unexpected impact of eliminating loss noted above. In APM lasers the normal understanding is that pulse width is set by soliton shaping, and pulse energy is set by the mode-locking parameters. The pulse width determines the degree of gain dispersion, and may be the physical cause of the memory integral in Equation 5-7. However, this is not born out by Figure 5-6, which shows the effect of changing the amplifier bandwidth. It would appear that the total area under the RIN curve is at most only weakly related to the degree of gain dispersion. In contrast, as seen in Figure 5-7 it is strongly related to the mode-locking parameter. Since the total gain in the mode-locking element is proportional to the integral of the pulse energy, the pulse reshaping could enter into the calculations through this element as well. Hence, mode-locking appears to be the most powerful parameter for controlling noise. The saturation term, γ_5, in particular appears to profoundly control the noise magnitude.

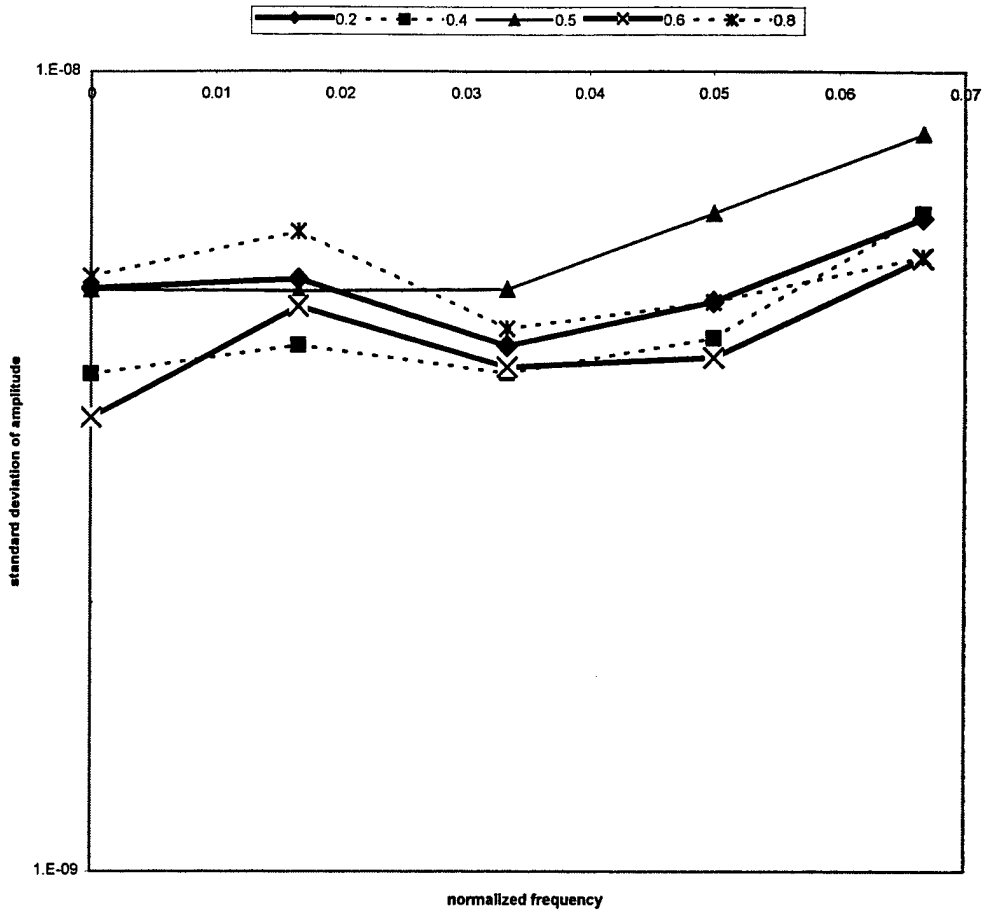

Figure 5-6 Shows variation in energy standard deviation with bin frequency for various amplifier bandwidths.

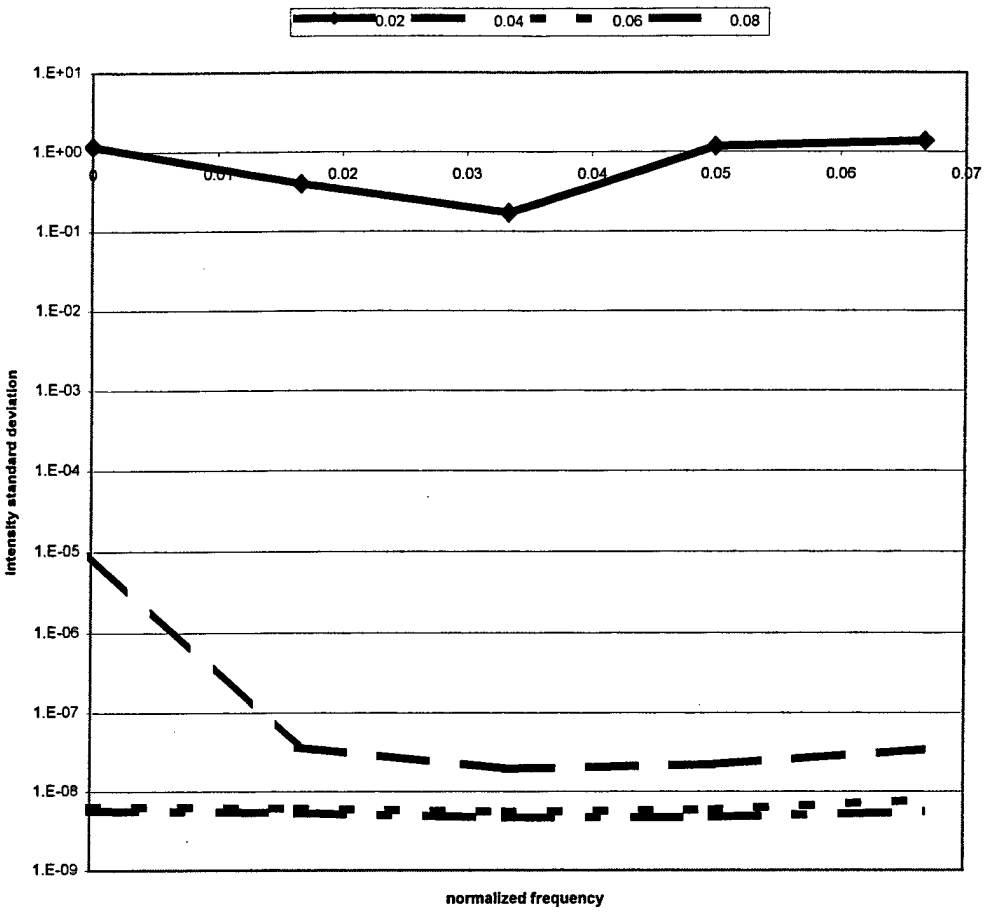

Figure 5-7 Shows variation in energy standard deviation with bin frequency for various mode-locking parameter values.

6 Conclusions

A detailed numerical model of mode-locked laser noise has been developed, and it has been used to derive noise spectra of RIN. It is found that there are new dynamics in this noise, which can be described using a damped harmonic oscillator model. The new effect does not appear to be brought about by gain dispersion, but rather by cavity loss and the presence of saturation in the mode-locking device. The saturation of the mode-locking action, represented by the parameter γ_5, appears to have the most effect. This suggests that control of γ_5 needs to be achieved to design low noise lasers. It also appears that there may be an optimum cavity loss for low noise operation.

7 References

[1] H. A. Haus and Antonio Mecozzi, "Noise of mode-locked lasers," *IEEE J. Quantum Electron.*, vol. 29, pp. 983-996, 1993.
[2] E. P. Ippen, H. A. Haus, and L. Y. Liu, "Additive pulse mode locking," *J. Opt Soc. Amer. B*, vol. 6, vol. 6, p. 1734, 1989.
[3] H. A. Haus, J. G. Fujimoto, and E. P. Ippen, "Structures for additive pulse mode locking," *J. Opt. Soc. Amer. B*, vol. 8, p. 2068, 1991.
[4] H. A. Haus, "Short Pulse Generation," in : *Compact Sources of Ultrashort Pulses*, ed. I.N. Duling III, (Cambridge Univ. Press, Cambridge, 1995) pp. 1-56.
[5] J. Theimer, M. Hayduk, M. F. Krol, and J. W. Haus, "Mode-locked Cr^{4+}:YAG laser: model and experiment," *Opt. Comm.*, vol. 142, pp. 55-60, 1997.
[6] J. Theimer, and J. W. Haus, "Figure-eight fibre laser stable operating regimes," *J. Mod. Opt.*, vol. 44, pp. 919-928, 1997.
[7] J. Theimer, and J. W. Haus, "Dispersion balanced figure-eight laser," *Opt. Comm.* vol. 34, p. 161, 1997.
[8] J. W. Haus, J. P. Theimer, R. L. Fork,"Polarization Distortion in Birefringent Fiber Amplifiers," *IEEE Photonics Tech. Lett.*, vol. 7, pp. 296-297, 1995.
[9] Govind P. Agrawal, *Nonlinear Fiber Optics 2nd ed."* (Academic Press, San Diego, 1995).
[10] A. Yariv, *Quantum Electronics 3rd ed.* , (Wiley, New York, 1989).
[11] H. A. Haus, Quantum noise in a solitonlike repeater system," *J. Opt. Soc. Am. B*, vol. 8, pp. 1122-1126, 1991.
[12] R. Loudon, *Quantum Theory of Light 2nd ed.*, (Oxford University Press, Oxford, 1983).
[13] A. Papoulis, *Probability, Random Variables, and Stochastic Processes 3rd ed.*, (McGraw-Hill, New York, 1991).
[14] D. F. Walls and G. J. Milburn, *Quantum Optics*, (Springer-Verlag, Berlin, 1994).
[15] B. E. A. Saleh and M. C. Teich, *Fundamentals of Photonics,* (Wiley, New York, 1991).
[16] J. P. Theimer, *Birefringent fiber devices and lasers,* Rome Laboratory Technical Report RL-TR-96-10, 1996.
[17]
[18] P. L. DeVries, *A First Course in Computational Physics,* (Wiley, New York, 1994).
[19] M. Sargent III, M. O. Scully, and W. E. Lamb, Jr., *Laser Physics*, (Addison Wesley, Reading, MA, 1974).
[20] M. O. Scully, and S. Zubairy, *Quantum Optics*, (Cambridge University Press, Cambridge, 1997).
[21] C. H. Henry, and R. F. Kazarinov, "Quantum noise in photonics," *Rev. Mod. Phys.*, vol. 68, pp. 801-853, 1996.
[22] S. Namiki, C. X. Yu and H. A. Haus, "Observation of nearly quantum-limited timing jitter in an all-fiber ring laser," *J. Opt. Soc. Am. B*, vol. 14, pp. 2817-2823, 1996.
[23] A. Papoulis, *Probability, Random Variables, and Stochastic Processes 3rd ed.,* (McGraw-Hill, New York, 1991).
[24] A. V. Oppenheim, and R. W. Schafer, *Discrete-Time Signal Processing,* (Prentice Hall, Englewood Cliffs, NJ, 1989).
[25] W. H. Press, S. A. Teukolsky, W. T. Vetterling, B. P. Flannery, *Numerical Recipes in C 2nd ed.,* (Cambridge University Press, Cambridge, 1992).
[26] Dr. Michael Hayduk, private communication.

DISTRIBUTION LIST

addresses	number of copies
AIR FORCE RESEARCH LABORATORY/SNDR JAMES P THEIMER 25 ELECTRONIC PKY ROME NY 13441-4515	5
ATTN: CHIEF SCIENTIST AFRL/IF 26 ELECTRONIC PKY ROME NY 13441-4514	1
AFRL/IFOIL TECHNICAL LIBRARY 26 ELECTRONIC PKY ROME NY 13441-4514	1
ATTENTION: DTIC-OCC DEFENSE TECHNICAL INFO CENTER 8725 JOHN J. KINGMAN ROAD, STE 0944 FT. BELVOIR, VA 22060-6218	2
BALLISTIC MISSILE DEFENSE ORGANIZATION 7100 DEFENSE PENTAGON WASH DC 20301-7100	2
AFRL/IFOIP 26 ELECTRONIC PKY ROME NY 13441-4514	1
RELIABILITY ANALYSIS CENTER 201 MILL ST. ROME NY 13440-8200	1
ATTN: GWEN NGUYEN GIDEP P.O. BOX 8000 CORONA CA 91718-8000	1

AFIT ACADEMIC LIBRARY/LDEE
2950 P STREET
AREA B, BLDG 642
WRIGHT-PATTERSON AFB OH 45433-7765 — 1

WRIGHT LABORATORY/MTM, BLDG 653
2977 P STREET, STE 6
WRIGHT-PATTERSON AFB OH 45433-7739 — 1

US ARMY SSDC
P.O. BOX 1500
ATTN: CSSD-IM-PA
HUNTSVILLE AL 35807-3801 — 1

NAVAL AIR WARFARE CENTER
WEAPONS DIVISION
CODE 4BL000D
1 ADMINISTRATION CIRCLE
CHINA LAKE CA 93555-6100 — 1

SPACE & NAVAL WARFARE SYSTEMS
COMMAND, EXECUTIVE DIRECTOR (PD13A)
ATTN: MR. CARL ANDRIANI
2451 CRYSTAL DRIVE
ARLINGTON VA 22245-5200 — 1

COR, US ARMY MISSILE COMMAND
REDSTONE SCIENTIFIC INFORMATION CTR
ATTN: AMSMI-RD-CS-R, DOCS
REDSTONE ARSENAL AL 35898-5241 — 2

ADVISORY GROUP ON ELECTRON DEVICES
SUITE 500
1745 JEFFERSON DAVIS HIGHWAY
ARLINGTON VA 22202 — 1

REPORT COLLECTION, CIC-14
MS P364
LOS ALAMOS NATIONAL LABORATORY
LOS ALAMOS NM 87545 — 1

AEDC LIBRARY
TECHNICAL REPORTS FILE
100 KINDEL DRIVE, SUITE C211
ARNOLD AFB TN 37389-3211 — 1

AFIWC/MSY
102 HALL BLVD, STE 315
SAN ANTONIO TX 78243-7016 1

NSA/CSS
K1
FT MEADE MD 20755-6000 1

AFRL/VSOS-TL (LIBRARY)
5 WRIGHT STREET
HANSCOM AFB MA 01731-3004 1

ATTN: EILEEN LADUKE/D460
MITRE CORPORATION
202 BURLINGTON RD
BEDFORD MA 01730 1

OUSD(P)/DTSA/DUTD
ATTN: PATRICK G. SULLIVAN, JR.
400 ARMY NAVY DRIVE
SUITE 300
ARLINGTON VA 22202 2

RICHARD PAYNE
AIR FORCE RESEARCH LAB/SNH
HANSCOM AFB, MA 01731-5000 1

JOSEPH P. LORENZO, JR.
AIR FORCE RESEARCH LAB/SNHC
HANSCOM AFB, MA 01731-5000 1

JOSEPH L. HORNER
AIR FORCE RESEARCH LAB/SNHC
HANSCOM AFB, MA 01731-5000 1

RICHARD A. SOREF
AIR FORCE RESEARCH LAB/SNHC
HANSCOM AFB, MA 01731-5000 1

ALBERT A. JAMBERDINO 1
AIR FORCE RESEARCH LAB/IFED
32 HANGAR RD
ROME NY 13441-4114

AIR FORCE RESEARCH LAB/SND 1
25 ELECTRONIC PKY
ROME NY 13441-4515

JOANNE L. ROSSI 1
AIR FORCE RESEARCH LAB/SNW
25 ELECTRONIC PKY
ROME NY 13441-4515

NY PHOTONIC DEVELOPMENT CORP 1
MVCC ROME CAMPUS
UPPER FLOYD AVE
ROME, NY 13440

ROBERT T. KEMERLEY 1
AIR FORCE RESEARCH LABORATORY/SND
2241 AVIONICS CIRCLE, RM C2G69
WRIGHT-PATTERSON AFB OH 45433-7322